

NOTE

^{19}F MRI of human lungs at 0.5 Tesla using octafluorocyclobutane

Olga S. Pavlova¹  | Nikolay V. Anisimov² | Lev L. Gervits³ | Mikhail V. Gulyaev²  |
Valentina N. Semenova¹ | Yury A. Pirogov¹ | Vladislav Ya. Panchenko¹

¹Faculty of Physics, Lomonosov Moscow State University, Moscow, Russia

²Faculty of Fundamental Medicine, Lomonosov Moscow State University, Moscow, Russia

³Nesmeyanov Institute of Organoelement Compounds of the Russian Academy of Sciences, Moscow, Russia

Correspondence

Olga S. Pavlova, Faculty of Physics,
Lomonosov Moscow State University,
Russia, 119991, Moscow, GSP-1, 1-2
Leninskiye Gory
Email: ofleup@mail.ru

Funding information

Russian Foundation for Basic Research,
Grant/Award Number: 17-02-00465 and
19-29-10015

Purpose: The aim of this study was to demonstrate the feasibility of fluorine-19 (^{19}F) MRI of the human lungs using octafluorocyclobutane (OFCB, C_4F_8). This gas has 8 magnetically equivalent fluorine nuclei and relatively long T_1 and T_2 (~50 ms), which render it suitable as an MRI contrast agent. Previous experiments in small laboratory animals showed that OFCB could be successfully used as an alternative to the gases often used for ^{19}F MRI (sulfur hexafluoride and perfluoropropane).

Methods: One male volunteer participated in this study. Immediately before an MRI scan, the volunteer inhaled the gas mixture—80% OFCB with 20% oxygen—and held his breath. Experiments were performed on a 0.5T whole-body MR scanner with a customized transmit–receive coil tuned at ^{19}F frequency. Fast spin echo in 2D and 3D modes was used for image acquisition. 2D images were obtained with in-plane resolution of $10 \times 10 \text{ mm}^2$ without slice selection. 3D images were obtained with the voxel size of $10 \times 10 \times 30 \text{ mm}^3$. Breath-hold duration was 20 s for 2D and 40 s for 3D imaging, respectively.

Results: Anatomically consistent ^{19}F MR images of the human lungs were obtained with SNR around 50 in 2D mode and 20 in 3D mode. 3D volumetric images of the lungs were reconstructed and provided physiologically reasonable volume estimates.

Conclusion: The application of OFCB enables informative ^{19}F lung imaging even at low magnetic field strengths. The OFCB gas shows promise as an inhalable contrast agent for fluorine lung MRI and has a potential for clinical translation.

KEYWORDS

^{19}F MRI, C_4F_8 , lung imaging, MRI of the human lungs, octafluorocyclobutane, OFCB

1 | INTRODUCTION

MRI of the human lung is generally difficult due to low proton density and short T_2 s caused by the porous structure of the organ. Conventional proton MRI with standard sequences is used to diagnose certain pulmonary conditions, such as

metastases and tumors, pneumonia, and pulmonary fibrosis.¹ The use of ultrafast sequences can further increase the sensitivity of proton MRI of the lungs.²

The diagnostic capabilities of lung MRI can be enhanced by using gases as inhalable contrast agents. The best results have been obtained to date with hyperpolarized noble gases (helium-3

and xenon-129).³⁻⁵ However, hyperpolarization methods are currently too expensive and complicated for routine clinical use.

Fluorinated gases can also be used as contrast agents. Compared to hyperpolarized inert gases, their production and use for MRI applications is simpler and cheaper. Due to 100% natural abundance of ^{19}F and large gyromagnetic ratio, which is only 6% less than that of the proton, fluorine MRI leads to comparable image SNR to proton MRI.

The absence of a background signal provides an additional advantage of fluorine-19 (^{19}F) over hydrogen -1 (^1H) MRI.

Most of inhalable fluorine contrast agents belong to the perfluorocarbon family, chemically synthesized compounds similar to hydrocarbons in which hydrogen is replaced by fluorine.^{6,7} These compounds are stable and biologically inert.

Lung MRI with a fluorinated gas was first performed in 1982.⁸ In that study, perfluoromethane (CF_4) was used to visualize the excised lungs of a rabbit. The first in vivo study of the rat lungs using perfluoroethane (C_2F_6) was carried out in 1998⁹ and the first ^{19}F MRI of the human lungs in 2008.¹⁰ In that study, sulfur hexafluoride (SF_6) was used as an inhalable contrast agent. The current fluorine MRI methods can be used to study lung ventilation function, gas diffusion, oxygen, partial pressure maps, etc.^{5,11,12}

SF_6 and perfluoropropane (C_3F_8) are the most frequently used gases for ^{19}F MRI¹³ due to their wide clinical applications, particularly in ophthalmological surgery and as ultrasound contrast agents.¹⁴⁻¹⁸ However, these gases are not ideal for MRI applications for 2 reasons: 1) C_3F_8 has a complex spectrum; and 2) SF_6 has very short relaxation times on the order of 1 to 2 ms.

Octafluorocyclobutane (OFCB, C_4F_8) was first proposed as a fluorine inhalable contrast agent in 2010 and tested for ^{19}F MRI of the pig lungs.¹⁹ This gas proved promising for ^{19}F MRI because it has 8 magnetically equivalent fluorine nuclei and relatively long relaxation times of several tens of milliseconds.

In our previous work,²⁰ we demonstrated the feasibility of using OFCB for in vivo visualization of the rat lungs at 7

T and compared its contrast properties with SF_6 .²⁰ In 2018, using this gas, we obtained 3D images of the entire rat respiratory system (lungs, trachea, and bronchi).²¹ Recently, Shepelytskyi et al²² used OFCB to visualize the rat lungs at 3 T.

This study demonstrates the application of OFCB as a contrast agent for MRI of the human lungs.

2 | METHODS

2.1 | MRI system

The experiments were performed on a custom-modified clinical 0.5T MR scanner Bruker Tomikon S50 (Bruker, Ettlingen, Germany). The system is equipped with a superconducting magnet (Magnex, Oxford, UK) with a bore diameter of 60 cm, 2 kW RF transmitter LPPA-2120 (Dressler, Stolberg, Germany), and gradient system S630 with 16.7 mT/m power and 0.5 ms rise time. The scanner is driven by open source software (XwinNmr v.1.0 and ParaVision 1.0) and can be tuned in a wide range of carrier frequencies (3-30 MHz), thus enabling multinuclear imaging and spectroscopy, including ^{19}F experiments.^{23,24}

For ^{19}F MRI, we modified the manufacturer's receive-only body coil (Part No. T5968, Figure 1A) to enable excitation and detection of the fluorine signal. In the original design, the coil is used for quadrature detection of the proton signal and consists of 2 orthogonal saddle coils. For fluorine MRI, 1 of the receiver channels was transformed to transmit–receive mode, enabling transmission of linearly polarized B_1 field, and both channels were tuned to the ^{19}F (19.8 MHz) resonance frequency at 0.5 T. The quality factor of an unloaded coil was approximately 200.

2.2 | Phantom experiments

As a phantom, we used a 3L plastic cylinder (Platypus, Seattle, USA) filled with either pure OFCB gas or the breathing mixture

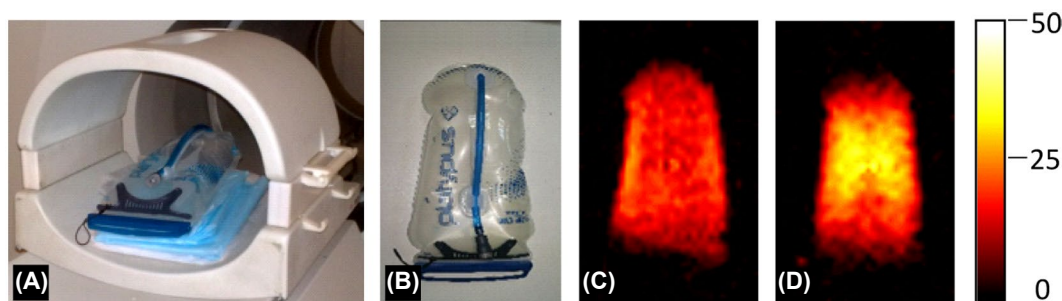


FIGURE 1 (A) Photograph of the ^{19}F MRI coil with the phantom inside. (B) Photograph of the phantom. (C and D) ^{19}F images of the phantom (SNR maps) in the coronal projection obtained using 2D GRE and FSE sequences, respectively. The color scale corresponds to SNR units. ^{19}F , fluorine-19; FSE, fast spin echo; GRE, gradient recalled echo

containing 80% OFCB and 20% oxygen. Figure 1A,B shows the phantom and its positioning inside the transceiver coil.

The ^{19}F relaxation times T_1 and T_2 were measured using nonselective inversion recovery and spin echo spectroscopy sequences, respectively. In these sequences, we used rectangular 90° and 180° RF pulses with 0.7 ms duration, the amplitudes of which differed by a factor of 2. The pulse width was calibrated by measuring the dependence of the ^{19}F spectral signal amplitude on the pulse duration using a single-pulse sequence. The inversion delay for T_1 measurements and TE for T_2 measurements varied from 5 to 300 ms, with TR = 1 s and the number of averages (NA) = 1.

^{19}F imaging of the phantom was performed using 2D gradient recalled echo (GRE) and fast spin echo (FSE) sequences with FOV = 25×40 cm and in-plane resolution 10×10 mm² (matrix 25×40). The sequences were executed with rectangular RF pulses and without a slice selection gradient.

The parameters for 2D GRE were TR/TE = 49/6 ms, flip angle = 90° , bandwidth = 4 kHz, and NA = 1. The parameters for 2D FSE were TR = 84 ms, echo spacing = 8 ms, echo train length = 4, bandwidth = 12 kHz, and NA = 2. With both sequences, a single slice image was acquired with the scan time of 1.3 s.

2.3 | In vivo MRI experiments

One healthy volunteer (male, 71 years old) participated in this study. The patient's height and weight were 190 cm and 105 kg, respectively. This study was approved by the institutional review board, and written informed consent was obtained prior to the study. The experimental procedure involved inhalation of the 80% OFCB and 20% oxygen gas mixture prior to each ^{19}F scan, followed by a breath-hold during image acquisition. Specifically, the volunteer took 3 deep breaths and exhalations from a 60 L plastic container with the gas mixture, and after the fourth inhalation (tidal volume breath) he held his breath for the duration of acquisition.

Before ^{19}F MRI, proton 2D GRE images of the chest in the coronal projection were obtained with the following parameters: FOV = 40×40 cm², matrix = 128×128 , 15 slices with 15 mm thickness, TR/TE = 415.2/7 ms, flip angle = 90° , NA = 2, scan time = 1 min 46 s.

^{19}F MRI of the human lungs was performed using the FSE sequence with a short echo train, which provided higher SNR as compared to GRE according to the results of phantom imaging detailed below. The FSE sequence was implemented with nonselective rectangular pulses with the duration of 1.5 ms. ^{19}F FSE images were acquired in the 2D and 3D modes with echo spacing = 8 ms, echo train length = 4, and bandwidth = 19.5 kHz. Single-slice 2D images were obtained in 3 orthogonal projections with 10 mm² in-plane resolution, FOV = 40×40 cm², matrix = 40×40 ,

TR = 69 ms, NA = 30, and scan time of 20 s. 3D FSE imaging was performed with voxel size of $1 \times 1 \times 3$ cm³, FOV = $40 \times 40 \times 24$ cm³, matrix = $40 \times 40 \times 8$, TR = 42 ms, NA = 12, and scan time of 40 s. To ensure that RF power deposition in human ^{19}F imaging is within safety limits, specific absorption rate was estimated using the formulas from Refs. ²⁵ and ²⁶ for the experimental sequence parameters (see Supporting Information 1). According to our calculations, specific absorption rate was about 0.57 W/kg, which is much less than the maximal permissible value within any national regulations.

2.4 | Image processing and analysis

Reconstruction of MR images was performed using proprietary software (ParaVision 1.0). To increase SNR about 2.5-fold for the images obtained with the 3D FSE sequence, k-space data were multiplied by the sine-squared function before 3D Fourier transform. This windowing function was used in 2 directions of the k-space, including the direction of frequency encoding.

ImageJ software was used for the subsequent image processing and analysis procedures, including superposition, reslicing, 3D rendering, volume estimation, and SNR calculation.²⁷ ^{19}F images were transformed into SNR maps in which SNR value in a given voxel (i, j) was computed as

$$SNR(i, j) = \frac{S(i, j) - S_N}{\sigma_N},$$

where $S(i, j)$ is the signal measured in a given voxel (i, j) of the image; S_N is the mean noise magnitude measured in a background region; and σ_N is the respective SD of noise from the same background region.

Lung volume was estimated from 3D FSE images using the Iterative Self-Organizing Data Analysis Technique algorithm²⁸ in ImageJ software based on an automatically determined intensity threshold.

3 | RESULTS

Relaxation measurements using the phantom showed that the T_1 and T_2 values were almost equal. For pure gas, $T_1 \approx T_2 = 53 \pm 4$ ms; and for the mixture of 80% OFCB and 20% oxygen, $T_1 \approx T_2 = 46 \pm 3$ ms.

^{19}F MR images of the phantom acquired using 2D GRE and FSE sequences are shown in Figure 1C,D. The FSE sequence demonstrated about a 20% to 30% SNR improvement as compared to the GRE sequence.

2D images of the human lungs in the 3 orthogonal projections are presented in Figure 2.

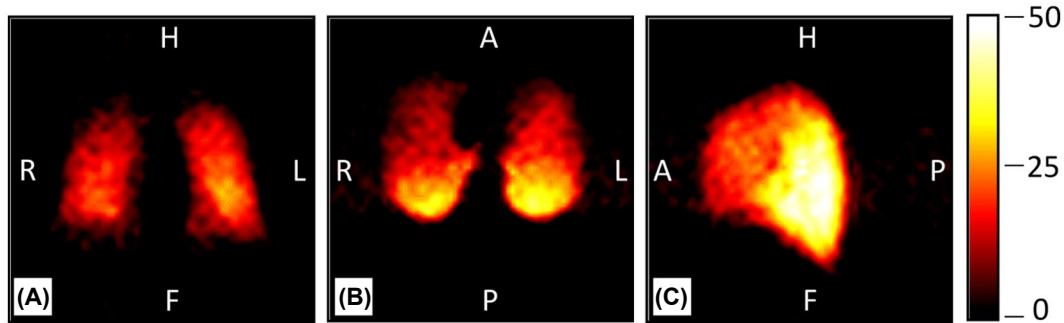


FIGURE 2 ^{19}F MRI SNR maps of human lungs obtained using the 2D FSE sequence without slice selection in the 3 orthogonal projections: (A) coronal, (B) axial, and (C) sagittal. The color scale corresponds to SNR units

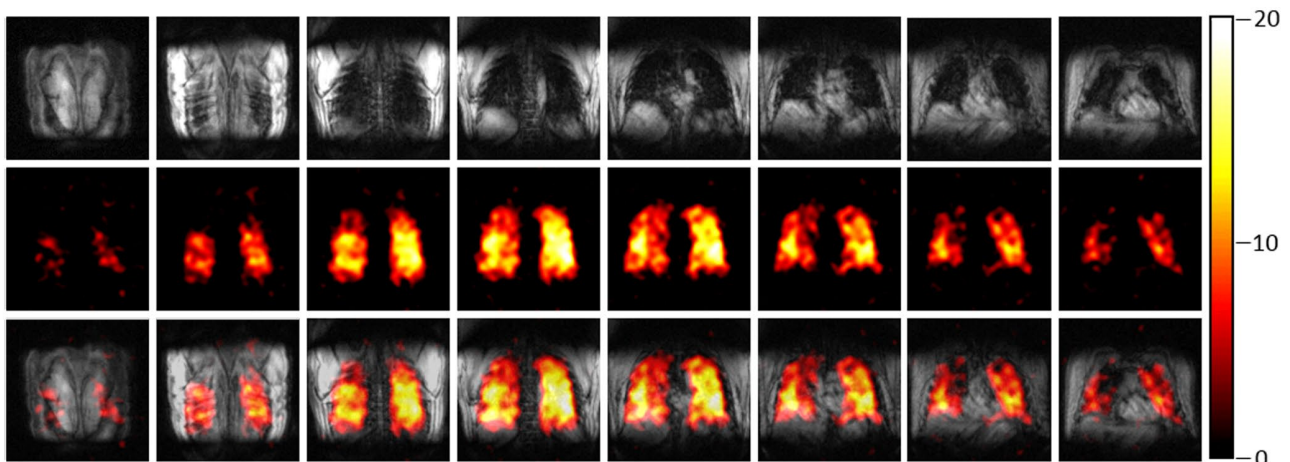


FIGURE 3 ^{19}F and ^1H MRI of human lungs. Top row: ^1H MRI (2D GRE); middle row: ^{19}F MRI SNR map obtained using 3D FSE; bottom row: superposition of ^1H and ^{19}F MRI. The color scale corresponds to SNR units. ^1H , hydrogen -1

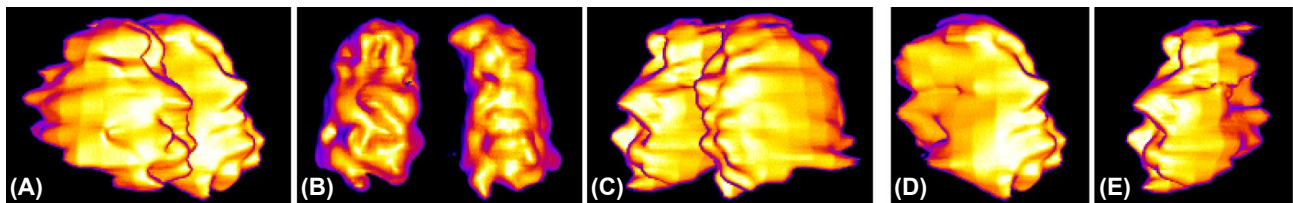


FIGURE 4 3D rendering of the human lungs obtained from 3D FSE images. (A, B, C) Images displaying both lungs; (D, E) images of the left and right lung displayed separately. Images are presented at the azimuthal viewing angles of -50° (A, D), 0° (B), and $+50^\circ$ (C, E)

Figure 3 (middle row) presents ^{19}F MRI of the human lungs obtained using 3D FSE sequence. It is shown as a series of slices in a coronal projection. The bottom row of Figure 3 represents the superposition of proton (top row) and fluorine images (middle row) obtained with the same spatial localization and confirms anatomical consistency of ^{19}F MR images. Maximal SNR values for in vivo images of the human lungs were around 50 and 20 for the 2D and 3D mode, respectively.

Figure 4A-C show volumetric images of the lungs (3D rendering) for 3 azimuthal viewing angles (50° , 0° , and $+50^\circ$) reconstructed from the 3D FSE image set. The volumes of the right and left lung were measured separately (Figure 4D,E). The volumes were 2.6 L and 2.4 L for the right and left

lung, respectively, which provide physiologically reasonable estimates.²⁹

4 | DISCUSSION

This study demonstrates the feasibility of in vivo human lung ^{19}F MRI with the use of OFCB as an inhalable contrast agent. Our results indicate that OFCB enables anatomically consistent lung imaging with high SNR even at low magnetic field strength. Taken together with previous reports,¹⁹⁻²² this study suggests that OFCB provides substantial advantages for in vivo lung MRI as compared to other inhalable fluorine contrast

agents. To our knowledge, the currently tested as ^{19}F contrast agents perfluorinated gases include perfluoromethane (CF_4), perfluoroethane (C_2F_6), SF_6 , C_3F_8 , and OFCB.^{8-12,29} Because the signal strength is proportional to the molar spin density,³⁰ the latter 2 compounds containing 8 fluorine atoms offer the highest value (0.35 mol/L).²⁹ Another important parameter affecting sensitivity of ^{19}F MRI is T_2 of the contrast agent because longer T_2 reduce unwanted signal decay during readout. Note that for gases, $T_2 \approx T_1$ therefore some T_2 estimates from the literature below are based on the actually measured T_1 values. The problem of extremely short T_2 (about 2 ms)²⁹ is the main limitation in the application of perfluoromethane and SF_6 gases. Among the above-mentioned perfluorinated agents, OFCB offers the longest T_2 value (around 46–47 ms), which is about 2.5-fold longer than T_2 of its closest competitor C_3F_8 (18 ms).²⁹ Of note, our relaxation measurements for OFCB appeared in excellent agreement with the literature data.²⁹ Finally, an important advantage of OFCB over C_3F_8 is magnetic equivalence of all fluorine nuclei in the molecule that results in a single-signal spectrum. In contrast, the C_3F_8 spectrum contains 2 signals originating from perfluorinated methyl and methylene groups, which may cause chemical shift artifacts and SNR loss without special techniques for spectrally selective excitation or detection.³¹

As a practical consequence of a long T_2 of OFCB, it was possible to apply the FSE sequence for in vivo ^{19}F imaging. Previous studies with other fluorine inhalable contrast agents³² employed various types of GRE sequences due to the requirement of very short TE. The FSE sequence offers improved SNR and reduced sensitivity to B_0 inhomogeneity and magnetic susceptibility artifacts, which is especially important for lung imaging due to the difference in magnetic susceptibilities between air and tissue.

One observation of this study is that the distribution of OFCB in the lungs appeared inhomogeneous in axial and sagittal projections (Figure 2B,C)—the closer to the back, the higher the MR signal. A similar pattern was also noted earlier,¹⁹ in which OFCB concentrated in the dorsal parts of the pig lungs. In addition to nonuniform gas penetration, there can be several explanations of this finding, including gravity, coil sensitivity profile, or the projection nature of the nonselective 2D technique used in this study. We believe that non-uniformity of signal distribution in the anterior-posterior direction on ^{19}F MR images of lungs is not due to gravity effect in OFCB because on axial and sagittal MR images of the phantom filled with this gas the signal distribution was relatively homogeneous (see Supporting Information Figure S1).

The application of the 3D FSE technique in our study resulted in images of acceptable quality (SNR up to 20), which allowed detection of the difference in the volumes of the right and left lungs. However, the breath-hold duration needed for 3D imaging appeared rather long (40 s), which exceeds clinical standards and may be prohibitive for patients with lung disease. Although a simple technical solution of this problem

could be multiple breath-hold or continuous-breathing respiratory-triggered acquisition,³²⁻³⁴ this approach would require a more advanced gas administration system, which was unavailable for this pilot study.

It is remarkable that our results were obtained at relatively low field of 0.5 T. Whereas this study highlights the current possibilities of low-field scanners for ^{19}F MRI of the human lungs, the use of high-field equipment offers certain advantages. Because the relatively long scan time in our experiments was caused by the need of signal averaging (12 for 3D FSE) to improve SNR, translation to higher magnetic fields is expected to alleviate this limitation. Additional capabilities of high-field MRI include the availability of accelerated although more SNR-demanding techniques, such as ultrashort TE,³⁵ parallel imaging,³⁶ and compressed sensing.³⁷ At the same time, direct translation of our imaging approach to higher magnetic fields may be difficult due to specific absorption rate limitations. Particularly, implementation of the FSE sequence with similarly short TR (about 40 ms) is unlikely to be possible at 3T or even at 1.5T in view of generally high RF power deposition delivered by this sequence. On the contrary, longer echo trains with reduced refocusing flip angles in combination with faster receivers and stronger gradients may enable a reasonable tradeoff for FSE imaging of the lungs with OFCB at high fields. Finally, it should be pointed out that particularly useful for high-field lung ^{19}F MRI GRE techniques employing mixed T1 and T2 contrast, such as SSFP,³⁸ would greatly benefit from the use of OFCB as a contrast agent.

5 | CONCLUSION

This study demonstrates that ^{19}F images of healthy human lungs can be acquired using OFCB at 0.5 T with a reasonable SNR, ranging from 20 to 50 for 3D and 2D acquisitions, respectively. The OFCB gas shows promise as an inhalable contrast agent for fluorine lung MRI and has a potential for clinical translation.

ACKNOWLEDGMENT

This work was supported by Russian Foundation for Basic Research grants 17-02-00465 and 19-29-10015.

ORCID

Olga S. Pavlova  <https://orcid.org/0000-0002-2574-1978>

Mikhail V. Gulyaev  <https://orcid.org/0000-0003-4684-2484>

REFERENCES

1. Biederer J, Beer M, Hirsch W, et al. MRI of the lung (2/3). Why ... when ... how? *Insights Imaging*. 2012;3:355-371.
2. Johnson KM, Fain SB, Schiebler ML, Nagle S. Optimized 3D ultrashort echo time pulmonary MRI. *Magn Reson Med*. 2013;70:1241-1250.

3. Sean Fain S, Schiebler ML, McCormack DG, Parraga G. Imaging of lung function using hyperpolarized helium-3 magnetic resonance imaging: review of current and emerging translational methods and applications. *J Magn Reson Imaging*. 2010;32:1398-1408.
4. Mugler JP, Altes TA. Hyperpolarized ^{129}Xe MRI of the human lung. *J Magn Reson Imaging*. 2013;37:313-331.
5. Kruger SJ, Nagle SK, Couch MJ, Yo O, Albert M, Fain SB. Functional imaging of the lungs with gas agents. *J Magn Reson Imaging*. 2016;43:295-315.
6. Tirotta I, Dichiarante V, Pigliacelli C, et al. F-19 magnetic resonance imaging (MRI): From design of materials to clinical applications. *Chem Rev*. 2015;115:1106-1129.
7. Ruiz-Cabello J, Barnett BP, Bottomley PA, Bulte JWM. Fluorine (F-19) MRS and MRI in biomedicine. *NMR Biomed*. 2011;24:114-129.
8. Heidelberger E, Lauterbur PC. Gas phase ^{19}F -NMR zeugmatography: a new approach to lung ventilation imaging. In Proceedings of the 1st Annual Meeting of SMRM, Boston, USA, 1982;70-71.
9. Kuethe DO, Caprihan A, Fukushima E, Waggoner RA. Imaging lungs using inert fluorinated gases. *Magn Reson Med*. 1998;39:85-88.
10. Wolf U, Scholz A, Terekhov M, et al. Fluorine-19 MRI of the lung: first human experiment. In Proceedings of the 16th Annual Meeting of ISMRM, Toronto, Canada. 2008;3207.
11. Fox MS, Gaudet JM, Foster PJ. Fluorine-19 MRI contrast agents for cell tracking and lung imaging. *Magn Reson Insights*. 2016;22;8(Suppl. 1):53-67.
12. Gutberlet M, Kaireit TF, Voskrebenev A, et al. Free-breathing dynamic ^{19}F gas MR imaging for mapping of regional lung ventilation in patients with COPD. *Radiology*. 2018;286:1040-1051.
13. Coucha MJ, Ballb IK, Lib T, et al. Inert fluorinated gas MRI: A new pulmonary imaging modality. *NMR Biomed*. 2014;27:1525-1534.
14. Sigler EJ, Randolph JC, Charles S, Calzada JI. Intravitreal fluorinated gas preference and occurrence of rare ischemic postoperative complications after pars plana vitrectomy: A survey of the American society of retina specialists. *J Ophthalmol*. 2012;2012; Article ID 230596. 5.
15. <https://imaging.bracco.com/us-en/products/contrast-enhanced-ultrasound/lumason> Accessed December 23, 2019.
16. Torres A, Koskinen SK, Gjertsen H, Fischler B. Contrast-enhanced ultrasound using sulfur hexafluoride is safe in the pediatric setting. *Acta Radiol*. 2017;58:1395-1399.
17. Hong Q, Cai R, Chen Q, et al. Three-dimensional HyCoSy with perfluoropropane-albumin microspheres as contrast agents and normal saline injections into the pelvic cavity for morphological assessment of the fallopian tube in infertile women. *J Ultrasound Med*. 2017;36:741-748.
18. <https://www.ec21.com/product-details/Perfluoropropane-Albumin-Microsphere-Injection-10625218.html> Accessed December 23, 2019.
19. Wolf U, Scholz A, Terekhov M, Koebrich R, David M, Schreiber LM. Visualization of inert gas wash-out during high-frequency oscillatory ventilation using fluorine-19 MRI. *Magn Reson Med*. 2010;64:1479-1483.
20. Pavlova OS, Volkov DV, Gulyaev MV, et al. Magnetic resonance imaging of the lungs on fluorine-19 nuclei with application of gas perfluorocyclobutane. *Meditinskaya Fizika*. 2017;4:59-64 (in Russian). <https://istina.msu.ru/publications/article/92562316/>
21. Pavlova OS, Semenova VN, Gulyaev MV, Gervits LL, Pirogov YA. Pirogov YuA Visualization of the laboratory animals respiratory system using ^{19}F MRI. *Journal of Radio Electronics (Zhurnal radioelektroniki) online journal*. ISSN 1684-1719, 2018;11:1-11 (in Russian).
22. Shepelytskyi Yu, Li T, Hane FT, et al. Octafluorocyclobutane as a novel ^{19}F MRI gas agent for significant lung image quality improvement. In Proceedings of the 27th Annual Meeting of ISMRM, Montreal, Canada. 2019. Abstract 1881.
23. Anisimov NV, Pavlova OS, Agafonnikova AG, Kosenkov AV, Fomina DV. Multinuclear applications on 0.5T magnetic resonance scanner. *Appl Magn Reson*. 2019;50:17-27.
24. Anisimov NV, Gulyaev MV, Volkov DV, Pavlova OS, Pirogov YA. Control of the radiofrequency field in fluorine (^{19}F) magnetic resonance imaging. *Phys Wave Phenom*. 2015;23:304-310.
25. Collins CM, Wang Z. Calculation of radiofrequency electromagnetic fields and their effects in MRI of human subjects. *Mag Reson Med*. 2011;65:1470-1482.
26. Plagenhoef S, Evans FG, Abdelnour T. Anatomical data for analyzing human motion. *Res Q Exerc Sport*. 1983;54:169-178.
27. Schneider CA, Rasband WS, Eliceiri KW. NIH image to ImageJ: 25 years of image analysis. *Nat Methods*. 2012;9:671-675.
28. Ridler TW, Calvard S. Picture thresholding using an iterative selection method. *IEEE Trans Sys Man Cyber*. 1978;8:630-632.
29. Kauczor, H-U (Ed.) *MRI of the Lung*. Berlin Heidelberg: Springer-Verlag; 2018;125-134, 173-176.
30. Toft P (Ed.) *Quantitative MRI of the Brain: Measuring Changes Caused by Disease*. Chichester: John Wiley & Sons; 2003;88.
31. Güden-Silber T, Temme S, Jacoby C, Flögel U. Biomedical ^{19}F MRI using perfluorocarbons. *Methods Mol Biol*. 2018;1718: 235-257.
32. Couch MJ, Ball IK, Li T, Fox MS, Biman B, Albert MS. ^{19}F MRI of the lungs using inert fluorinated gases: Challenges and new developments. *J Magn Reson Imaging*. 2019;49:343-354.
33. Ahmed F, Halaweish AF, Cecil Charles HC. Physiorack: An integrated MRI safe/conditional, gas delivery, respiratory gating, and subject monitoring solution for structural and functional assessments of pulmonary function. *J Magn Reson Imaging*. 2014;39:735-741.
34. Klimeš F, Voskrebenev A, Gutberlet M, et al. Free-breathing quantification of regional ventilation derived by phase-resolved functional lung (PREFUL) MRI. *NMR Biomed*. 2019;32:e4088.
35. Couch MJ, Ball IK, Li T, et al. Pulmonary ultrashort echo time ^{19}F MR imaging with inhaled fluorinated gas mixtures in healthy volunteers: Feasibility. *Radiology*. 2013;269:903-909.
36. Deshmane A, Gulani V, Griswold MA, Seiberlich N. Parallel MR imaging. *J Magn Reson Imaging*. 2012;36:55-72.
37. Neal MA, Pippard BJ, Hollingsworth KG, et al. Optimized and accelerated ^{19}F -MRI of inhaled perfluoropropane to assess regional pulmonary ventilation. *Magn Reson Med*. 2019;82:1301-1311.
38. Maunder A, Rao M, Robb F, Wild JM. Optimization of steady-state free precession MRI for lung ventilation imaging with ^{19}F C3F8 at 1.5T and 3T. *Magn Reson Med*. 2019;81:1130-1142.

SUPPORTING INFORMATION

Additional supporting information may be found online in the Supporting Information section.

FIGURE S1 ^{19}F MRI SNR maps of phantom obtained using 2D FSE in coronal (A), axial (B) and sagittal (C) projections; D, E – SNR plot profiles in the anterior-posterior direction (yellow lines on B and C) of axial and sagittal projections, respectively. The color scale corresponds to SNR units

How to cite this article: Pavlova OS, Anisimov NV, Gervits LL, et al. ^{19}F MRI of human lungs at 0.5 Tesla using octafluorocyclobutane. *Magn Reson Med*. 2020;84:2117–2123. <https://doi.org/10.1002/mrm.28270>